Appl. Phys. B 82, 183–188 (2006)
DOI: 10.1007/s00340-005-2066-0

Applied Physics B
Lasers and Optics

M. WOLLENHAUPT✉
A. PRÄKELT
C. SARPE-TUDORAN
D. LIESE
T. BAUMERT

Quantum control by selective population of dressed states using intense chirped femtosecond laser pulses

University of Kassel, Institute of Physics and Center for Interdisciplinary Nanostructure Science and Technology (CINSaT), Heinrich-Plett-Straße 40, 34132 Kassel, Germany

Received: 1 August 2005/Revised version: 19 October 2005
Published online: 17 December 2005 • © Springer-Verlag 2005

ABSTRACT The physical mechanism of strong field quantum control using chirped femtosecond laser pulses is investigated. Dressed state control is exerted by making explicit use of the temporal phase changes of the pulse. In our experiment, the dressed state population is mapped by photoelectron spectra from simultaneous excitation and ionization of potassium atoms as a function of the chirp parameter. We show that chirped pulses can be used to selectively steer ground state atoms temporarily into a single dressed state realizing transient Selective Population of Dressed States (SPODS).

PACS 32.80.Qk; 32.80.Rm; 33.80.Rv

1 Introduction

Quantum control using shaped femtosecond laser pulses has opened up numerous fascinating perspectives in fundamental and applied research [1–4]. Applications range from physical chemistry, non-linear optics and quantum information to the control of light harvesting in bio-molecules. The unique coherence properties of femtosecond laser pulses enable to exert quantum control experiments with full control over the electrical field in terms of phase, amplitude and polarization. The realm of strong field quantum control beyond the perturbative regime has become accessible by high pulse intensities delivered by ultrashort pulses with only moderate pulse energy. Because intense fields enable the richest controlled dynamics, investigations of strong field quantum control are triggered by fundamental interest and the prospect to design more efficient pulse shapes once the mechanisms are better understood. In the spirit of this direction, in this contribution, we investigate the light induced dynamics of a model system (potassium atoms) using intense phase modulated laser pules.

Generally, weak field quantum control concepts are no longer valid when the perturbative description of the light matter interaction breaks down. However, it was demonstrated that weak-field coherent control principles to manipulate the final state population are applicable to non-perturbative control employing so called real electric fields, i.e. resonant shaped pulses which are purely amplitude modulated in time domain [5]. This implies that the pulse envelope has a constant temporal phase except for π-jumps which merely represent a change of the sign of the envelope. For example, pulses subjected to third order dispersion (TOD) are real, whereas linearly chirped pulses with group delay dispersion (GDD) are not real in that sense. As a consequence, pulses with phase discontinuities or gradual changes of the temporal phase present a challenging regime to analyze.

We extend this concept to strong field control of transient amplitudes which take the key position in approaching the final population in realistic multistep control processes. A suitable physical model to describe the interaction of intense laser fields with matter is provided by dressed states [6], i.e., the eigenstates of the Hamiltonian, which includes the laser-matter interaction. In the context of transient amplitudes it is the selective population of dressed states (SPODS) that provides selectivity in a multistep control scenario. However, there is no selective population of dressed states using real pulses of arbitrary shape. This aspect is illustrated in Fig. 1 on the photoelectron spectra resulting from a resonant structured real laser pulse generated by modulation in frequency domain. Generally, photoelectron spectroscopy is used to map the bare states of an atomic or molecular system. However, when the ionization field coincides with the excitation field, the field-dressed states are probed. In Fig. 1a phase modulation (TOD) is used whereas amplitude modulation (spectral hole at the transition frequency) is used in Fig. 1b. Despite the highly structured pulse shape, the Autler–Townes (AT) [7] doublet in the photoelectron spectrum is symmetrical, which implies that both dressed states are equally populated. This is a general property of real pulses, because the excited state amplitude $c_b(t)$ is always purely imaginary during the light matter interaction and hence the photoelectron spectrum – which arises from the Fourier transform of $c_b(t)E^2(t)$ (see (1)) – is always symmetrical. As a consequence, strong field control of the dressed state population requires control of the transient amplitudes using fields which exhibit temporal phase changes.

An example of strong field control on the AT-doublet in the photoelectron spectrum using interferometric double pulse sequences, i.e., pulses featuring phase discontinuities, was reported in [8] and interpreted in terms of the dressed state control in [9, 10]. Alternatively, phase jumps generated by sinusoidal phase modulation were employed to control the

✉ Fax: +49 561 804 4453, E-mail: wollenha@physik.uni-kassel.de

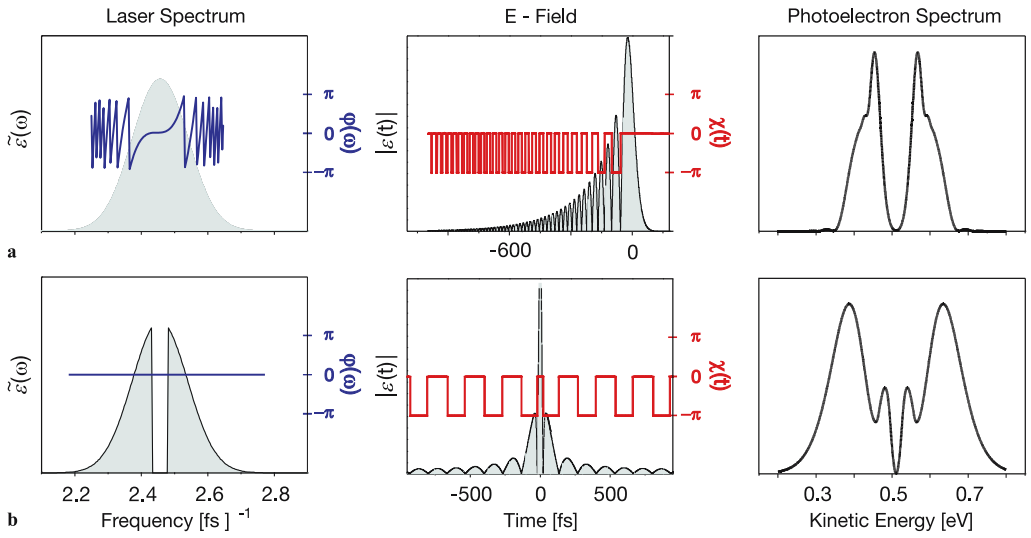

FIGURE 1 Photoelectron spectra resulting from (**a**) phase- or (**b**) amplitude modulated pulses. *Left*: modulated laser spectra $\tilde{\mathcal{E}}(\omega)$ and the spectral phase function $\varphi(\omega)$ (phase wrapped), *middle*: temporal laser electric field envelope $\mathcal{E}(t)$ and temporal phase $\chi(t)$, *right*: corresponding photoelectron spectra. Despite the complicated pulse shapes, no selectivity of the dressed state population is achieved by real pulses

dressed state population [11]. In contrast to the abrupt change of the temporal phase in those experiments, in this contribution, we demonstrate how chirped pulses featuring continuous frequency sweeps, can be used to control SPODS. To this end we measure kinetic photoelectron spectra as a function of the chirp introduced by a quadratic phase modulation function in frequency domain [12, 13]. Chirped laser pulses play a very prominent role in quantum control theoretically and experimentally [14–20].

The paper is organized as follows. First we describe the theoretical treatment (Sect. 2), then the experimental setup is briefly described (Sect. 3). Experimental results are presented in Sect. 4. The physical mechanism is discussed in Sect. 5.

2 Theoretical description

Figure 2 shows the excitation scheme used in this experiment. Unlike conventional pump-probe scenarios in which the first pump pulse initiates the dynamics, which is probed by a second pulse in our experiment, a single chirped pulse is used to drive the dynamics in the neutral atoms and also to simultaneously ionize the $4p$ atoms. Our experiments are described theoretically by iteratively solving the time dependent Schrödinger equation (TDSE) [21, 22] for the (linearly polarized) light induced neutral atomic dynamics in order to consider strong field effects. In our simulations potassium atoms are described by a three-level system ($4p_{1/2} \leftarrow 4s$ and $4p_{3/2} \leftarrow 4s$) weakly coupled to a flat continuum, i.e., photoionization is treated using perturbation theory since the neutral-to-ionic transitions are much weaker than for instance the K ($4p \leftarrow 4s$) transitions. The amplitudes $c(\omega_e)$ for photoelectrons with kinetic energy $\hbar\omega_e$ generated by the two-photon ionization from the $4p$ excited state read [23–25]

$$c(\omega_e) \propto \int_{-\infty}^{\infty} c_{4p}(t) E^2(t)\, e^{i(\omega_e+\omega_{IP}-\omega_{4p})t}\, dt\,, \qquad (1)$$

where $c_{4p}(t)$ describes the time dependent amplitude of the $4p$ state with the energy $\hbar\omega_{4p}$ and $\hbar\omega_{IP}$ is the ionization energy. The electric field $E(t) = \mathcal{E}(t)\, e^{i\omega_0 t}$ can be decomposed into the (complex) envelope $\mathcal{E}(t)$ and the carrier $e^{i\omega_0 t}$ with the laser frequency ω_0 detuned from the atomic resonance by $\delta = \omega_{4p\leftarrow 4s} - \omega_0$. The envelope contains the temporal phase $\chi(t)$ and can be written as $\mathcal{E}(t) = |\mathcal{E}(t)|\, e^{i\chi(t)}$. In Sect. 5 the dynamics are discussed in a simplified picture. In that section we use resonant chirped excitation of a two-level system for clarity. The dressed state amplitudes $(d_{low}(t), d_{up}(t))$ are obtained from the bare state amplitudes $(c_a(t), c_b(t))$ using the unitary transformation [26]

$$\begin{pmatrix} e^{-i\chi/2}\cos(\Theta) & e^{i\chi/2}\sin(\Theta) \\ -e^{-i\chi/2}\sin(\Theta) & e^{i\chi/2}\cos(\Theta) \end{pmatrix}, \qquad (2)$$

with the mixing angle Θ

$$\tan(2\Theta) = \frac{|\Omega|}{\delta} \qquad (3)$$

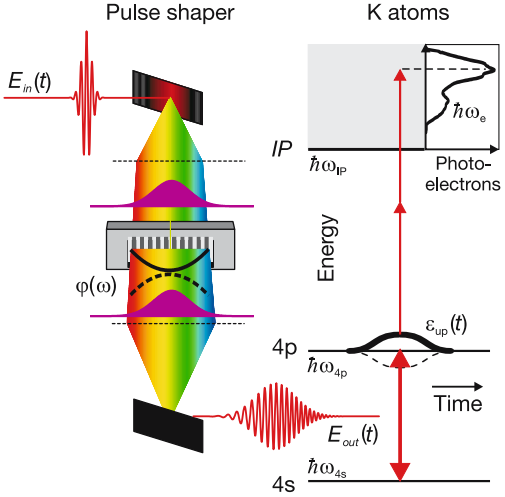

FIGURE 2 Excitation scheme (*right*) and schematic experimental setup (*left*). Ultrashort 30 fs laser pulses from a titanium-sapphire amplifier $E_{in}(t)$ are sent into a 128 pixel liquid crystal spatial light modulator. Quadratic phase functions $\varphi(\omega)$ produce chirped pulses $E_{out}(t)$ which are used for simultaneous excitation and ionization of potassium atoms. Due to the non-stationary temporal phase a single dressed state is populated during the interaction as indicated with the *bold line* in the atomic level scheme. Energy resolved photoelectron spectra probe the transient dressed state population for different chirp parameters φ_2

determined by the Rabi frequency Ω and the detuning δ. The bare state amplitudes $c_a(t)$ and $c_b(t)$ obtained from the solution of the TDSE are used to construct the Bloch vector [27]

$$\boldsymbol{\rho}(t) = \begin{pmatrix} c_a^* c_b + c_a c_b^* \\ i\left(c_a^* c_b - c_a c_b^*\right) \\ |c_b|^2 - |c_a|^2 \end{pmatrix} . \quad (4)$$

The dynamics in the Bloch picture is described by $\dot{\boldsymbol{\rho}}(t) = \boldsymbol{\Omega_B}(t) \times \boldsymbol{\rho}(t)$ with the angular velocity vector in the frame rotating with the laser frequency

$$\boldsymbol{\Omega_B} = \begin{pmatrix} -|\Omega| \cos(\chi) \\ -|\Omega| \sin(\chi) \\ \delta \end{pmatrix} . \quad (5)$$

3 Experimental setup

Femtosecond laser pulses (30 fs full-width at half maximum, 788 nm central wavelength) from a Ti:sapphire amplifier were phase modulated by a home-built pulse shaper [28] (see Fig. 2), containing a 128 pixels liquid crystal spatial light modulator. In this experiment, we applied quadratic spectral phase modulations $\varphi(\omega) = \frac{\varphi_2}{2}(\omega - 2.4\,\mathrm{fs}^{-1})^2$ at the pulse shaper to generate chirped pulses. The modulated pulses were focussed by a 300 mm fused silica lens into a vacuum chamber (1.3×10^{-6} mbar) to intersect a potassium atomic beam. Solid potassium was heated up to 360 °C in an oven chamber with an exiting nozzle of 200 μm diameter, connected to the vacuum chamber. The photoelectrons from multiphoton ionization were detected using a magnetic bottle spectrometer, yielding time-of-flight spectra (see Fig. 2) which are converted into kinetic energy photoelectron spectra. We calibrated the magnetic bottle spectrometer with a Nd:YAG (532 nm) and a dye laser (548 nm and 570 nm) by ionizing the xenon $5p_{1/2}$ and $5p_{3/2}$ ground states as well as the potassium ground state $4s_{1/2}$. In the experiment, the pulse energy was set to 0.5 μJ. We measured a beam waist radius of 30 μm for the femtosecond laser in the interaction area with a cutting knife method, resulting in an intensity of about 6×10^{11} W/cm^2.

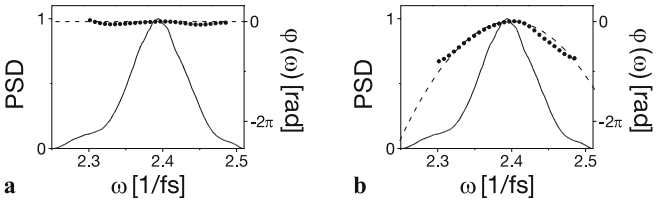

FIGURE 3 Quadratic spectral phases set by the pulse shaper and retrieved by a Grenouille. *Solid lines* show the normalized power spectral density (PSD) recorded by a spectrometer. The *dashed lines* show simulated spectral phases. The *dots* represent spectral phases measured by a Grenouille. In case (**a**), no spectral phase modulation was applied at the pulse shaper while in (**b**) φ_2 was set to -500 fs^2. In both cases, an uncompensated group delay dispersion of -140 fs^2 was subtracted

The dispersion introduced by the fused silica focussing lens and the fused silica entrance window of the vacuum chamber was pre-compensated with the help of the prism compressor of the Ti:sapphire amplifier. We adjusted the prism compressor such that the femtosecond pulses were bandwidth-limited at a Grenouille [29] after passing through an equivalent thickness fused silica plate. Moreover, the phase introduced by the pulse shaper was occasionally measured with the Grenouille. In Fig. 3, simulated and measured spectral phases are depicted for a quadratic spectral phase modulation. Fig. 3a depicts the case of no phase modulation while in b a quadratic phase modulation of $\varphi_2 = -500$ fs^2 was applied. Good agreement between the measurement and the simulation is observed showing the fidelity of the phase modulation.

4 Experimental results

Figures 4a and b show false color representations of the simulated and measured photoelectrons with the chirp parameter φ_2 ranging from -1900 fs^2 (down chirp) to $+1900$ fs^2 (up chirp). Depending on the chirp either slow or fast photoelectrons are observed demonstrating selective population of the lower or the upper dressed state. The

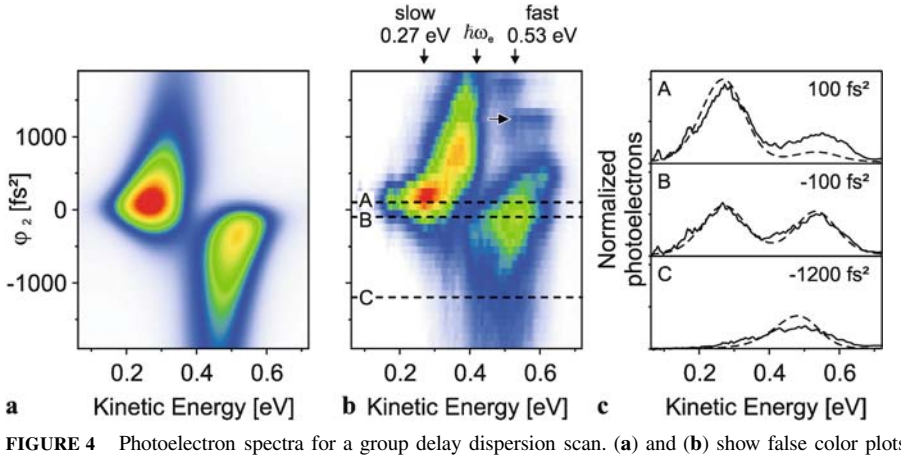

FIGURE 4 Photoelectron spectra for a group delay dispersion scan. (**a**) and (**b**) show false color plots of simulated (**a**) and measured (**b**) photoelectron spectra. For each group delay dispersion φ_2 a photoelectron spectrum was recorded. In the simulation, a 30 fs Gaussian pulse at 788 nm was applied. The *vertical arrows* in (**b**) are at the energies of the slow and fast photoelectrons as well as at the excess energy $\hbar\omega_e$. The *horizontal dashed lines* in (**b**) indicate the positions of the photoelectron spectra separately shown in (**c**): (A) 100 fs^2, (B) -100 fs^2 and (C) -1200 fs^2, with either the lower (A), upper (C) or both (B) dressed states populated (measured: *solid lines*, simulated: *dashed lines*). Note that the additional maximum at around 1250 fs^2, 0.6 eV indicated with a *horizontal arrow* in (**b**) arises from a spectral phase discontinuity at the transition frequency due to phase wrapping within the pulse shaper

comparison between the experimental results and the simulations shows reasonable agreement. Since the laser frequency $\omega_0 = 2.4\ \mathrm{fs}^{-1}$ is slightly detuned from the resonance frequency $\omega_{ba} = 2.45\ \mathrm{fs}^{-1}$, the AT spectrum is not quite symmetrical even for a bandwidth limited pulse ($\varphi_2 = 0$). Because the laser is red detuned the slow photoelectrons are slightly more pronounced.

Photoelectron spectra at specific φ_2 are presented in Fig. 4c. These photoelectron spectra were extracted at (A) $\varphi_2 = 100\ \mathrm{fs}^2$ (slight up-chirp), (B) $-100\ \mathrm{fs}^2$ (slight down chirp) and (C) $-1200\ \mathrm{fs}^2$ (strong down chirp) from the photoelectron distributions in Fig. 4a and b. The results shown in Fig. 4 clearly demonstrate our ability to control the dressed states population via the chirp parameter: up-chirped laser pulses prepare the selective population of the lower dressed state (see Fig. 4c case A), whereas down-chirped pulses prepare the selective population of the upper dressed state (see Fig. 4c case C). Setting the chirp parameter to $-100\ \mathrm{fs}^2$ results in approximately equal population of both dressed states. The slight down-chirp, therefore, compensates the effect of the detuning of the laser frequency with respect to the atomic transition. Our results show that continuous changing the temporal phase using chirped pulses allows to steer ground state atoms into a preselected dressed state with high selectivity.

5 Discussion

In order to present a physical picture of the underlying mechanism we describe our experimental observations in terms of a simplified model containing two approximations. First potassium atoms are described as two level atoms and second resonant excitation is considered. For excitation we use a 30 fs Gaussian laser pulse modulated by a quadratic spectral phase function. Fig. 5a shows the pulse envelope, which is significantly broadened (187 fs FWHM of the intensity) due to the $-2000\ \mathrm{fs}^2$ down-chirp and the corresponding quadratic temporal phase function $\chi(t)$. For the sake of clarity, a chirp parameter of $-2000\ \mathrm{fs}^2$ was chosen to illustrate the physical mechanism in the limit of large chirp parameters. This value is a lower limit for our measurement (cf. Fig. 4). The time evolution of the bare state population (Fig. 5b) reveals that for large chirp parameters the physical mechanism converges to Rapid Adiabatic Passage (RAP) [19, 30]. Note that the RAP is insensitive to the direction of the chirp and, thus, the bare state population is not influenced by the sign of the chirp. Observation of the bare state population is, therefore, not sufficient to explain the alternating photoelectron spectra. Initially, the dressed states are equally populated as shown in Fig. 5c. During the excitation process, the upper dressed state population increases leading to the (transient) selective population of the upper dressed state during the time interval of maximum intensity of the laser pulse (see Fig. 5c). At the maximum laser intensity, the dressed states are split by 0.1 eV as seen in Fig. 5d. Since the probability for ionization is highest during this time interval only photoelectrons from the upper dressed state are observed in the photoelectron spectrum (compare with Fig. 4c case C) and therefore the transient selective population is mapped. In contrast to the bare state population, the dressed state population is sensitive to the sign of the chirp. For an up-chirped laser pulse, the population of the dressed states is reversed (not shown) leading to (transient) selective population of the lower dressed state. The photoelectron spectrum therefore consists of a single peak at low kinetic energies as observed experimentally (see Fig. 4c case A). Bandwidth limited laser pulses show no selectivity, i.e., both dressed states are equally populated during the laser matter interaction leading to a symmetric photoelectron spectrum similar to the experimental observation presented in Fig. 4c case B.

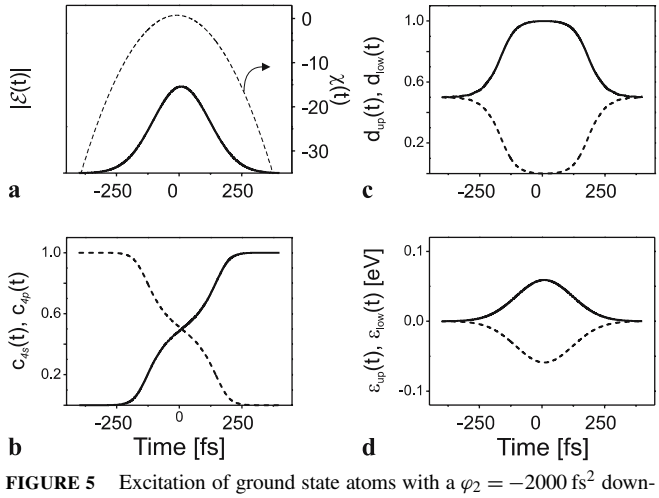

FIGURE 5 Excitation of ground state atoms with a $\varphi_2 = -2000\ \mathrm{fs}^2$ down-chirped pulse. (**a**) pulse envelope $|\mathcal{E}(t)|$ and the temporal phase $\chi(t)$ (*dashed*), (**b**) time evolution of the bare state population $c_{4s}(t)$ (*dashed*) and $c_{4p}(t)$, (**c**) time evolution of the dressed state population $d_{\mathrm{up}}(t)$ and $d_{\mathrm{low}}(t)$ (*dashed*) and (**d**) energy of the dressed states $\varepsilon_{\mathrm{up}}(t)$ and $\varepsilon_{\mathrm{low}}(t)$ (*dashed*)

We now discuss the physical mechanism of chirped excitation in the Bloch picture in the resonant case, i.e., without detuning $\delta = 0$ (see Fig. 6). The Bloch picture is particularly suitable to analyze the dynamics because it provides a link between bare state and dressed state dynamics. In addition, since the interplay of the optical phase and the quantum mechanical phase are visualized we can use this picture to understand the mechanism of SPODS exerted by phase discontinuities [9, 10] and pulses with continually varying phases. In the frame rotating with the laser frequency ω_0 (see left hand parts of Fig. 6), the angular velocity vector $\boldsymbol{\Omega_B}$ remains in the u, v plane and chirped excitation is characterized by the rotation of $\boldsymbol{\Omega_B}$ in the u, v plane due to the time dependent optical phase $\chi(t)$. For down-chirped (up-chirped) pulses, the rotation of $\boldsymbol{\Omega_B}$ in the u, v plane changes from counter-clockwise (clockwise) to clockwise (counter-clockwise) around the $+w$ axis when the instantaneous laser frequency passes the resonance (time zero). At this time, i.e., at the equator, the Bloch vector $\boldsymbol{\rho}(0\ \mathrm{fs})$ is parallel to the angular velocity vector $\boldsymbol{\Omega_B}(0\ \mathrm{fs})$ for down-chirped pulses (see Fig. 6 lower panel). Whenever the Bloch vector and the angular velocity vector are parallel the upper dressed state is selectively populated in agreement with the temporal evolution of the dressed state population shown in Fig. 5c. This demonstrates again how chirped pulses lead to transient SPODS. For up-chirped pulses, $\boldsymbol{\rho}(0\ \mathrm{fs})$ is antiparallel to $\boldsymbol{\Omega_B}(0\ \mathrm{fs})$ at the equator, corresponding to the selective population of the lower dressed state (see Fig. 6 upper panel).

In the frame rotating with the instantaneous laser frequency $\omega(t)$ where the optical phase vanishes at all times

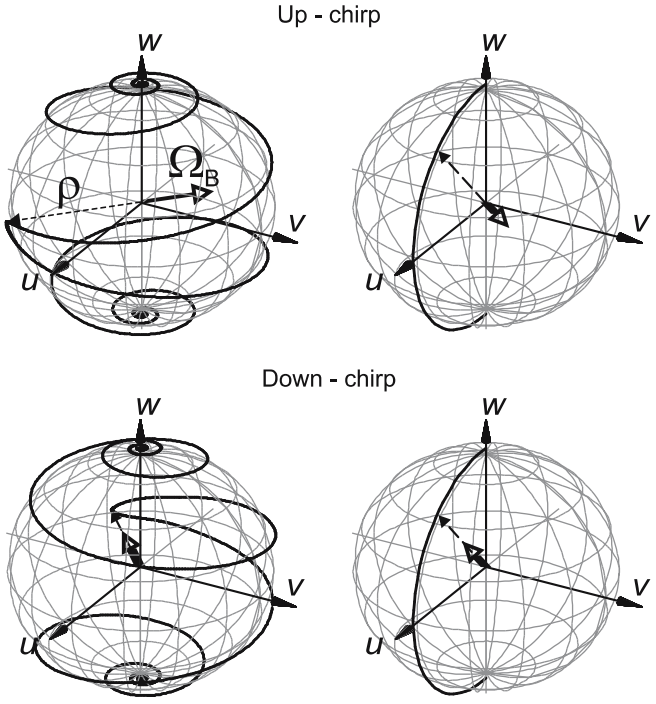

FIGURE 6 Bloch sphere representation of strong field excitation for an up-chirped pulse (*upper panel*) and a down-chirped pulse (*lower panel*). *Left*: frame rotating with the laser frequency ω_0 *right*: frame rotating with instantaneous frequency $\omega(t)$. For up-chirped pulses the Bloch vector $\boldsymbol{\rho}$ (*dashed arrow*) and angular velocity vector $\boldsymbol{\Omega_B}$ (*open arrow head*) are temporarily anti-parallel in the frame rotating with ω_0 indicating the transient selective population of the lower dressed state. In the frame rotating with $\omega(t)$ both vectors are always anti-parallel due to adiabatic following. Down-chirped pulses lead to parallel vectors $\boldsymbol{\rho}$ and $\boldsymbol{\Omega_B}$ indicating the transient selective population of the upper dressed state

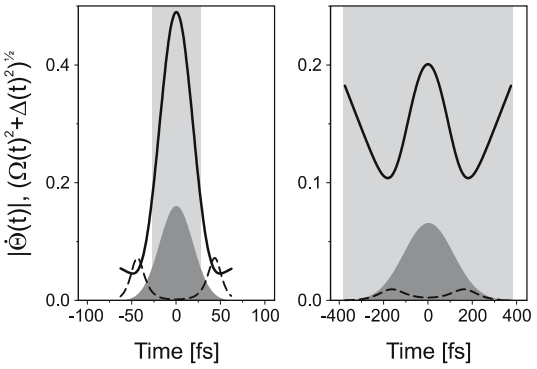

FIGURE 7 Time dependence of the adiabatic condition. Comparison of the time derivative of the mixing angle $|\dot{\Theta}(t)|$ (*dashed line*) and the (generalized) Rabi frequency $\sqrt{\Omega(t)^2+\Delta(t)^2}$ (*solid line*) for $\phi_2 = 100\,\mathrm{fs}^2$ (*left*) and $\phi_2 = 2000\,\mathrm{fs}^2$ (*right*). The *dark shaded curve* shows the respective laser electrical field $|\mathcal{E}(t)|$. Note the different scaling of the axes in both graphs. The *light grey shaded area* indicates the interval in which the adiabaticity factor $Q > 10$, i.e. the adiabatic condition is (approximately) met

the chirp is expressed in terms of a time-dependent detuning $\Delta(t) = \dot{\chi}(t)$ (see right hand parts of Fig. 6). We illustrate how transient SPODS converges to RAP for large chirps. For a down-chirped pulse (up-chirped) $\boldsymbol{\Omega_B}$ initially points to the south (north) pole and moves smoothly to the north (south) pole. In both cases the Bloch vector initially points to the south pole. In this picture the Bloch vector adiabatically follows the angular velocity vector [31] being approximately parallel (anti-parallel) during the whole process (Fig. 6 lower (upper) panel). Finally, we note that for transient SPODS the adiabatic condition $|\dot{\Theta}(t)| \ll \sqrt{\Omega(t)^2+\Delta(t)^2}$ [19, 26, 32] needs to be fulfilled only during the most intense part of the pulse. As an illustration, the time dependence of $|\dot{\Theta}(t)|$ and the (generalized) Rabi frequency $\sqrt{\Omega(t)^2+\Delta(t)^2}$ are depicted in Fig. 7 for the chirp parameters $\phi_2 = 100\,\mathrm{fs}^2$ and $\phi_2 = 2000\,\mathrm{fs}^2$. It is seen that for small chirp parameters ($\phi_2 = 100\,\mathrm{fs}^2$) the adiabatic condition is violated in the wings of the laser pulse, i.e., $|\dot{\Theta}(t)| > \sqrt{\Omega(t)^2+\Delta(t)^2}$. However, during the central part of the pulse – where ionization is most probable – the time dependent adiabaticity factor $Q(t)$ [32] defined by

$$Q(t) = \frac{\sqrt{\Omega(t)^2+\Delta(t)^2}}{|\dot{\Theta}(t)|} \tag{6}$$

exceeds a value of 10 as indicated by the grey shaded area in Fig. 7. For large chirp parameters ($\phi_2 = 2000\,\mathrm{fs}^2$) $Q(t)$ exceeds 10 during the whole process confirming that SPODS converges to RAP in the limit of large chirps. Since SPODS is also observed for small chirp parameters, we conclude that – in contrast to RAP – the mechanism of SPODS can be realized even if the adiabatic condition is not fulfilled during the complete excitation process.

6 Summary

In this paper we presented a study of photoelectron spectra resulting from simultaneous excitation and ionization using intense chirped femtosecond pulses. Our results were discussed in the bare state picture, the dressed state picture and the Bloch vector model. In order to present a physical picture of this strong field control mechanism we exploited the connection between these pictures. The dressed state picture delivers a very natural explanation of the experimental observations. In strong laser fields, photoelectron spectra map the dressed state population and hence the observation of a single AT component indicates SPODS. In the Bloch picture SPODS occurs when the Bloch vector $\boldsymbol{\rho}$ and the angular velocity vector $\boldsymbol{\Omega_B}$ are (anti-) parallel. In view of quantum control, the question of controllability of the photoelectron spectrum in strong laser fields was addressed. Since real pulses do not allow the dressed state population to be manipulated, pulses featuring a change of the temporal phase were used to exert control on the dressed state population. Besides earlier realizations of SPODS by phase jumps [8–11], we demonstrate here how chirped pulses – which are characterized by a continuous change of the temporal phase – can be used to selectively steer ground state atoms (temporarily) into a single dressed state. In particular up-chirp pulses populate the lower dressed state and vice versa. Unlike RAP, SPODS by chirped pulses can be used for quantum control of transient processes even if the adiabatic condition is not fulfilled during the whole process. Because many different pulse shapes exist which realize SPODS, we believe that SPODS is an important physical mechanism in the realm of strong field quantum control.

ACKNOWLEDGEMENTS The support of the Deutsche Forschungsgemeinschaft and the NRC-Helmholtz program are gratefully acknowledged.

REFERENCES

1 H. Rabitz, R. de Vivie-Riedle, M. Motzkus, K. Kompa, Science **288**, 824 (2000)
2 S.A. Rice, M. Zhao, *Optical Control of Molecular Dynamics* (Wiley-Interscience, New York 2000)
3 M. Shapiro, P. Brumer, *Principles of the Quantum Control of Molecular Processes*, (Wiley-Interscience, Hoboken 2003)
4 T. Brixner, T. Pfeifer, G. Gerber, M. Wollenhaupt, T. Baumert, Kluwer Series on Progress in Lasers: Femtosecond Laser Spectroscopy, ed. by P. Hannaford, Chapt. 9: Optimal Control of Atomic and Molecular and Electron Dynamics with Tailored Femtosecond Pulses, (2004)
5 N. Dudovich, T. Polack, Avi Pe'er, Y. Silberberg, Phys. Rev. Lett. **94**, 083 002-1 (2005)
6 C. Cohen-Tannoudji, J. Dupont-Roc, G. Grynberg, *Atom-Photon Interactions, Basic Processes and Aplications*, (John Wiley, New York 1992)
7 S.H. Autler, C.H. Townes, Phys. Rev. **100**(2), 703 (1955)
8 M. Wollenhaupt, A. Assion, O. Bazhan, C. Horn, D. Liese, C. Sarpe-Tudoran, M. Winter, T. Baumert, Phys. Rev. A **68**, 015 401 (2003)
9 M. Wollenhaupt, V. Engel, T. Baumert, Annu. Rev. Phys. Chem. **56**, 25 (2005)
10 M. Wollenhaupt, A. Präkelt, C. Sarpe-Tudoran, D. Liese, T. Baumert, J. Opt. B: Topical issue on quantum control **7** S270 (2005)
11 M. Wollenhaupt, A. Präkelt, D. Liese, C. Sarpe-Tudoran, T. Baumert, J. Mod. Opt. **52**, 2187 (2005)
12 J.C. Diels, W. Rudolph, *Ultrashort Laser Pulse Phenomena*, (Academic Press, San Diego, 1996)
13 M. Wollenhaupt, A. Assion, T. Baumert, Femtosecond Laser Pulses: Linear Properties, Manipulation, Generation and Measurement, In: *Springer Handbook of Lasers and Optics*, (Springer 2006) in press
14 P. Balling, D.J. Maas, L.D. Noordam, Phys. Rev. A **50**(5), 4276 (1994)
15 C.J. Bardeen, Q. Wang, C.V. Shank, Phys. Rev. Lett. **75**(19), 3410 (1995)
16 V.V. Lozovoy, S.A. Antipin, F.E. Gostev, A.A. Titov, D.G. Tovbin, O.M. Sarkisov, A.S. Vetchinkin, S.Y. Umanskii, Chem. Phys. Lett. **284**, 221 (1998)
17 M.A. Bouchene, C. Nicole, B. Girard, J. Phys. B **32**(21), 5167 (1999)
18 A. Assion, T. Baumert, J. Helbing, V. Seyfried, G. Gerber, Chem. Phys. Lett. **259**, 488 (1996)
19 N.V. Vitanov, T. Halfmann, B.W. Shore, K. Bergmann, Annu. Rev. Phys. Chem. **52**, 763 (2001)
20 G.P. Djotyan, J.S. Bakos, G. Demeter, P.N. Ignacz, M.A. Kedves, Z. Sörlei, J. Szigeti, Z.L. Toth, Phys. Rev. A **68**, 053 409-1 (2003)
21 B.M. Garraway, K.A. Suominen, Rep. Prog. Phys. **58**, 365 (1995)
22 A. Präkelt, M. Wollenhaupt, C. Sarpe-Tudoran, T. Baumert, Phys. Rev. A **70**, 063 407-1 (2004)
23 H.H. Bebb, A. Gold, Phys. Rev. **143**(1), 1 (1966)
24 C. Meier, V. Engel, Phys. Rev. Lett. **73**(24), 3207 (1994)
25 D. Meshulach, Y. Silberberg, Phys. Rev. A **60**(2), 1287 (1999)
26 Bruce W. Shore, *The Theory of Coherent Atomic Excitation, Volume 1: Simple Atoms and Fields*, (John Wiley New York 1990)
27 R.P. Feynman, F.L. Vernon, R.W. Hellwarth, J. Appl. Phys **28**, 49 (1957)
28 A. Präkelt, M. Wollenhaupt, A. Assion, C. Horn, C. Sarpe-Tudoran, M. Winter, T. Baumert, Rev. Sci. Instrum. **74**(11), 4950 (2003)
29 P. O'Shea, M. Kimmel, X. Gu, R. Trebino, Opt. Lett. **26**, 932 (2001)
30 D. Goswami, Phys. Rep. **374**, 385 (2003)
31 L. Allen, J.H. Eberly, *Optical Resonance and Two-Level Atoms*, (Dover Publications, New York, dover books on physics edition, 1987)
32 J. Baum, R. Tycko and A. Pines, Phys. Rev. A **32**(6), 3435 (1985)